Rapid Damage Scenario Assessment for Earthquake Emergency Management

Valerio Poggi*[1], Chiara Scaini[1], Luca Moratto[1], Gabriele Peressi[2], Paolo Comelli[1], Pier Luigi Bragato[1], and Stefano Parolai[1]

Abstract

The rapid availability of reliable damage statistics, after the occurrence of a major earthquake, is an essential mitigation strategy to drive and support emergency intervention operations. Unfortunately, the latency in collecting and organizing actual damage information has a substantial impact on the efficiency of the initial phases of the intervention framework. To speedup preliminary management operations, a quick, although, coarse prediction of the expected damage is highly desirable.

For this purpose, we have developed a system for rapid damage estimation. The system, presently implemented for the Friuli Venezia Giulia region, relies on the existing seismological monitoring infrastructure of the National Institute of Oceanography and Applied Geophysics (OGS), which is responsible for delivering earthquake alerts in northeastern Italy.

In case of a major earthquake event, the predicted damage is automatically computed using the OpenQuake software engine by means of ad hoc structural exposure and fragility models developed for the region. Damage calculations rely on a combination of actual observed ground motion from the stations of the OGS seismological network and empirical prediction using the ShakeMaps software developed by the U.S. Geological Survey. The resulting damage scenario, aggregated at municipality level, is finally delivered to the control room of the regional civil protection in support of early intervention activities.

Although, the system is presently still under active development, a number of experimental trials have confirmed the reliability and the usefulness of the proposed approach. We are confident that the current research will contribute in mitigating the impact of possible future damaging earthquakes by (1) guiding targeted postevent emergency interventions, (2) increasing the preparedness and response capacity of emergency teams and population through preparatory training activities, and (3) supporting the decision-making process during the recovery phase, hence enhancing resilience.

Introduction

Earthquakes represent one of the major natural threats worldwide, and their impact on population is often exacerbated by high vulnerability of the built environment. In this regard, efficient and effective risk mitigation strategies involve the implementation and application of adequate engineering prevention measures, including the enforcement of appropriate seismic design and the retrofitting of existing exposed structures to sustain the expected seismic hazard level. Complementary to preemptive actions, impact on population can also be mitigated by adopting efficient postevent intervention strategies, involving the coordination of emergency operations and the implementation of adequate recovery measures. As a matter of fact, time is critical when facing a severe earthquake crisis, and focused intervention is key to limit losses and casualties. Unfortunately, as the damage might be distributed unevenly on the stroke area, the major obstacle, in this sense, is the limited availability of information in the first tens of minutes after the event, to drive emergency teams and to guide the decision-making process.

To overcome the problem, a common strategy is to train specialized operators onsite (e.g., voluntary public servants from municipalities or local institutions) to rapidly report, in case of emergency, information about damage, casualties, service interruption, and so forth, on the territory. Although, this approach proved to be useful (Goretti and Di Pasquale, 2004; Cimellaro

1. National Institute of Oceanography and Applied Geophysics—OGS, Udine, Italy; 2. Civil Protection of the Friuli Venezia Giulia Region, Udine, Italy

*Corresponding author: vpoggi@inogs.it

et al., 2014; Dolce and Goretti, 2015), it is still affected by a rather large latency, which makes it of limited applicability in the early stages of intervention. Moreover, collecting, organizing, and summarizing such information for the use of decision makers is often problematic, because it involves a level of technical interpretation (Cimellaro *et al.*, 2014).

A suitable alternative approach consists in the prediction of the expected damage distribution, solely based on numerical or empirical models (or a mixture of the above). In this case, the overall latency is just due to the calculation time, which, however, strictly depends on the model complexity. The system needs, therefore, to be adapted and optimized to the level of being practically useful, often at the expense of the prediction accuracy, to increase responsiveness. Nonetheless, additional constraints can always be added a posteriori to the prediction, as soon as new information becomes progressively available, to increase the robustness of the estimate. Noticeable examples of the application of this strategy can be found in Erdik *et al.* (2003), Bal *et al.* (2008), and Borzi *et al.* (2019). Examples of such frameworks are also available for the United States (HAZUS methodology developed by the U.S. Federal Emergency Management Agency [FEMA], HAZUS, 1999), Europe (Risk-UE project, Mouroux and Le Brun, 2006), and at national scale (e.g., the Italian platform Italian Risk Map [IRMA], Borzi, Onida, *et al.*, 2020, and references therein).

The Seismological Research Centre (CRS) is a department of the National Institute of Oceanography and Applied Geophysics (OGS) in Italy. Founded after the devastating M_L 6.4 earthquake that struck the Friuli region in 1976, the CRS is responsible for the maintenance of the monitoring networks and the collection of seismological data in northeastern Italy. The dense seismological network (Priolo *et al.*, 2005; Bragato *et al.*, 2011), consisting nowadays in over 40 stations, including short-period, broadband and accelerometric sensors, allows accurate automatic locations of seismic events within seconds (Moratto and Sandron, 2015). The CRS section has also the mandate to support the regional civil protection (PCR) activities in Friuli Venezia Giulia (FVG) and Veneto: during emergencies, CRS issues alerts (Bragato and Govoni, 2000), event solutions (magnitude, location, focal mechanism), and preliminary ground-shaking estimates using the U.S. Geological Survey (USGS) ShakeMaps properly calibrated on the monitored area (Moratto *et al.*, 2009, 2011).

During the last decades, research activities at CRS have been mainly focused on seismological aspects, producing a wide amount of valuable scientific knowledge for the region (e.g., Bressan *et al.*, 2003; Bragato, 2009; Slejko *et al.*, 2011; Sugan and Peruzza, 2011; Bressan *et al.*, 2016). Such information is paramount but, without a proper evaluation of the impact of the earthquake on buildings and population, it might be insufficient to guide emergency intervention after catastrophic events and, more, in general, for the mitigation of damage through preventive land and urban planning.

With the goal of not only improving preparedness to strong damaging earthquakes, but also of better understanding the impact of specific earthquake scenarios on buildings and population, CRS is developing a system for rapid damage scenario assessment (RDSA). The system, presently operational for the FVG region, is closely integrated to the seismic monitoring networks of OGS, from which it receives event solutions and ground-motion information as inputs for the prediction. In case of a large, potentially damaging event, the system automatically produces an evaluation of the number of residential buildings, aggregated at municipality level, subject to severe damage (levels D4–D5 according to European Macroseismic Scale 1998 [EMS-98]; Grünthal, 1998). The damage scenario is then delivered to the control room of the PCR, to support local coordination of early intervention operations.

In this article, we illustrate the main technical characteristics of the RDSA system and its practical use for the purpose of reducing the impact of future earthquakes on the territory monitored by the CRS. In the first part, special attention is given to the description of the modeling strategies implemented for the different components (ground-motion hazard, structural fragility, and regional exposure) required to generate a realistic damage scenario. Subsequently, the main operational assumptions and the results of a preliminary validation exercise are discussed thoroughly, to highlight the applicability and main limitations of the proposed calculation schema for the purpose of civil protection and emergency planning.

Damage Assessment Methodology

The quantification of the earthquake impact on the built environment and population is done by evaluating three main components: the earthquake hazard (H), the distribution of the exposed assets (E), and their associated vulnerability (V). These elements, together, depict the seismic risk (R) of the study area. Specifically, if the damage on structures and infrastructures (D) is concerned, the vulnerability is more properly described by the use of structural fragility models (F).

Earthquake hazard can be broadly defined as the severity of any physical phenomenon associated to seismic activity and with potential to cause harm. Among others, ground shaking is, by far, the most relevant effect, due to its direct impact on the natural (e.g., landslides, ground failure) and built (e.g., collapse of structures, service interruption) environments. The ground-shaking potential of a site can be evaluated by quantifying the ground-motion level expected to be reached or exceeded after an earthquake of given characteristics, chosen (1) as more likely or the best representative (deterministic seismic hazard assessment [DSHA]; Kramer, 1996) or (2) from an ensemble of many possible alternative scenarios, each with a given probability of occurrence (probabilistic seismic hazard assessment [PSHA]; Cornell, 1968). In fact, DSHA and PSHA share several similarities (Bommer, 2002), whereas, the major difference consists in accounting or not for the temporal dependency of the

earthquake phenomenon to occur. Nowadays, due to performance improvements of the seismological networks and technological development of the processing techniques, the most relevant earthquake information (e.g., magnitude, location, source geometry, and orientation) is readily available a few seconds after the occurrence of any major event. For the purpose of rapidly characterizing the associated ground shaking, a scenario-based hazard assessment is, therefore, necessary. ShakeMap software (Wald *et al.*, 1999) is a popular tool developed by USGS, to portray the ground-shaking distribution following a potentially damaging earthquake. The software can be integrated into the alert system of an existing seismological monitoring network, making it a suitable tool for rapid scenario definition.

While earthquake hazard quantifies the natural phenomenon per se, structural exposure describes the number, typology (e.g., masonry, reinforce concrete, steel frame), and spatial distribution of the assets affected by the earthquake, such as residential buildings, infrastructures, or critical facilities. Exposure data can be collected by a number of direct or indirect sources, including national census or remote sensing (e.g., Wieland *et al.*, 2012). However, the definition of spatial and temporal variability of exposure is a complex task, and the quality of the data strongly influences the results of loss assessment (Bal *et al.*, 2010; Dell'Acqua *et al.*, 2013). For regional studies, building inventory information is usually aggregated at the level of province, municipality, or other smaller of administrative divisions (e.g., boroughs, census units), distinguishing between residential and nonresidential typologies.

Complementary to exposure information, fragility depicts the response of these elements to the ground shaking. It is usually expressed by the probability of exceeding a target damage state (e.g., slight, moderate or heavy damage on structural elements, total collapse) in a given building typology subject to a specific earthquake ground-motion level (e.g., Crowley *et al.*, 2004). Here, we adopt the common EMS classification of seismic-induced damages on buildings (Grünthal, 1998) that identifies five levels (D1–D5) of increasing damage (negligible-to-slight, moderate, substantial-to-heavy, very heavy, and destruction).

Fragility models can be derived empirically by laboratory experiments or by analyzing available damage information from actual earthquake events (e.g., Rota *et al.*, 2008; De Luca *et al.*, 2015; Del Gaudio *et al.*, 2017; Rosti *et al.*, 2018; Masi *et al.*, 2019), or analytically by means of numerical models simulating the dynamic behavior of buildings (e.g., Borzi, Crowley, and Pinho, 2008; Borzi, Pinho, and Crowley, 2008; Vona, 2014; Donà *et al.*, 2020; Milosevic *et al.*, 2020). An exhaustive compendium of fragility functions that can be adopted for the European building stock has been collected within the global earthquake model (GEM) project (see Data and Resources, Yepes-Estrada *et al.*, 2016), for which fragility functions can be downloaded in a format that can be directly used by the OpenQuake (OQ) tools.

The structural damage associated to a specific earthquake scenario can then be predicted by combining the expected (or measured) ground motion with precompiled exposure and fragility information for the study area.

Damage Model Setup

Ground-motion hazard scenario using ShakeMaps

ShakeMap (Worden *et al.*, 2020) is a software package that allows a rapid evaluation of the ground-motion distribution after an earthquake; version 4.0 has been recently released, with improvements focused principally on new interpolation algorithm (Worden *et al.*, 2018). Although, ShakeMap provides just a rough empirical estimate, based on the use of ground-motion prediction equations (GMPEs), the ground shaking can be locally conditioned by instrumentally recorded data from stations of the seismic network and using site-specific amplification models.

The ShakeMap 4.0 system has been implemented in northeastern Italy by OGS, linked on real-time data acquired by CRS and other neighboring seismic networks (see Data and Resources). In agreement with Istituto Nazionale di Geofisica e Vulcanologia (INGV) recommendations for the Italian territory, OGS adopts Italian configuration by Michelini *et al.* (2020) for strong earthquakes ($M_L \geq 4.0$); in case of weaker events ($M_L < 4.0$), the ShakeMaps are generated using the GMPE proposed by Massa *et al.* (2008) for northern Italy. The availability of dense seismic networks is fundamental to constrain the ground-motion estimations, especially in near-field area (Moratto *et al.*, 2009), in which the near-source effects are likely less captured by the adopted GMPEs. As an example, Figure 1 shows a ShakeMap generated for a moderate earthquake (M_L 3.9) with triggered recording stations.

Using the ShakeMap software, the ground-motion distribution is evaluated using different intensity measures (IMs), including peak ground acceleration (PGA), peak ground velocity (PGV), macroseismic intensity (derived from PGA using the conversion relation by Faenza and Michelini, 2010, 2011), and 5% critically damped response spectra (SA) for several periods (0.3, 1.0, and 3.0 s). For the purpose of a rapid damage assessment, we presently use PGA, which is a common choice among the existing fragility studies. Some authors show that PGA is suitable for buildings (e.g., Del Gaudio *et al.*, 2017; Rosti *et al.*, 2018) but can give good results also for bridges (Zelaschi *et al.*, 2019). However, others show that PGV is more suitable for unreinforced masonry (URM, Zucconi *et al.*, 2020). According to some authors, PGA, PGV, and SA are, in general, suitable for structures with periods lower than 2 s (Palanci and Senel, 2019). Overall, there is still a strong debate around the choice of the appropriate IM (Silva *et al.*, 2019), thus affecting the reliability of the estimated fragility functions and, as a consequence, of the assessed damage scenario (Ciano *et al.*, 2020). Further work is needed to include fragility curves that make use of different IMs (as suggested by Silva *et al.*, 2019) and to calibrate the model accordingly. We are presently investigating the possibility of including other spectral ordinates, in combination with ad

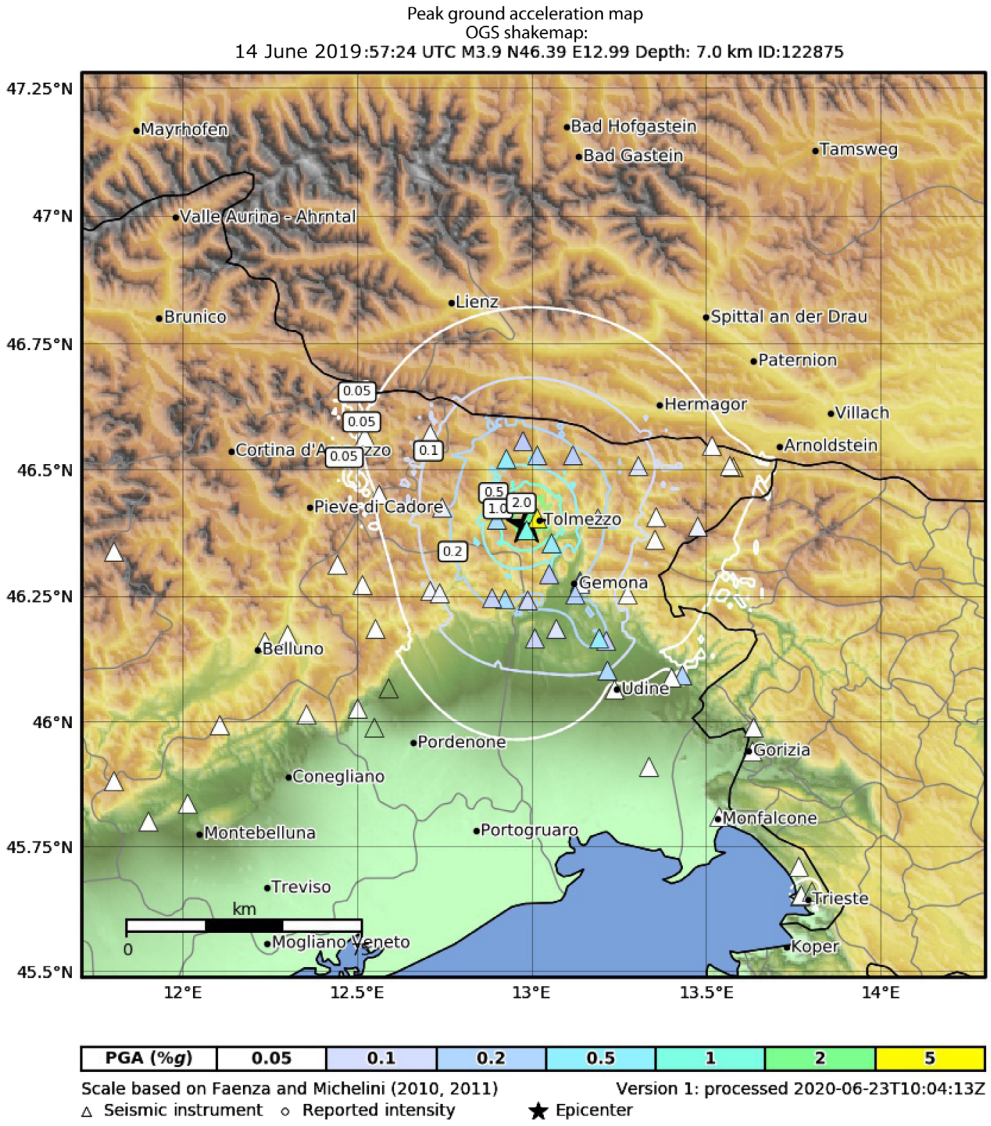

Figure 1. Example of ShakeMap for an earthquake (M_L 3.9) occurred in Friuli Venezia Giulia (FVG) region. The star shows the epicenter, whereas, the triangles show the recording stations. Ground motion is peak ground acceleration (PGA) in percentage of gravity (percent *g*). The color version of this figure is available only in the electronic edition.

hoc developed fragility functions and exposure that account for building specific response (e.g., empirically determined fundamental frequencies).

Exposure model

The structural exposure model for the FVG region is, primarily, derived from the information available in the census database (2011) of the Italian National Institute of Statistics (ISTAT), which provides, for each census unit, the geographical location and the number of buildings with indication of the age (either creation or renovation), building material, and number of floors. Based on the ISTAT classification, we identified 27 main typological classes that are the combination of three building material types (URM, reinforced concrete [RC], and a generic unclassified type name other), four age classes (except for type other), and three storeys classes. Though, it must be noted that the ISTAT description of the different building characteristics is rather coarse, which imposed a very general and broad typological classification scheme in our model. Targeted studies are, nonetheless, presently ongoing, with the aim of better characterizing the most representative building typologies for the region.

By analyzing the spatial distribution of residential buildings in the region (Fig. 2), it is evident that a large number of buildings is located in the main cities (Trieste, Udine, Pordenone, and Gorizia), while a relatively small fraction is located in the alpine area (northern part of the region). The most common and widespread building typology is URM, followed by RC, which is dominant in urban areas and in those municipalities damaged by the Friuli 1976 earthquake (highlighted on the map). Figure 3 shows the percentage of buildings for each building material, age class, and number of storeys: a high percentage of buildings in the FVG region has been constructed after the Second World War (1945–1970) and during the 1970–1990 period, respectively, during the Italian economic boom, which gave rise to a rapid development of the construction industry, and in the post-1976 reconstruction.

Selection of structural fragility models

To depict the failure conditions of the most common residential building typologies in the FVG region, we have selected a number of suitable fragility models from the existing literature and open datasets such as that of the European Systemic Seismic Vulnerability and Risk Assessment of Complex Urban, Utility, Lifeline Systems and Critical Facilities (SYNER-G) project (SYNER-G, 2009) and the GEM fragility curves database (Yepes-Estrada *et al.*, 2016). The appropriate fragility models were identified, based on

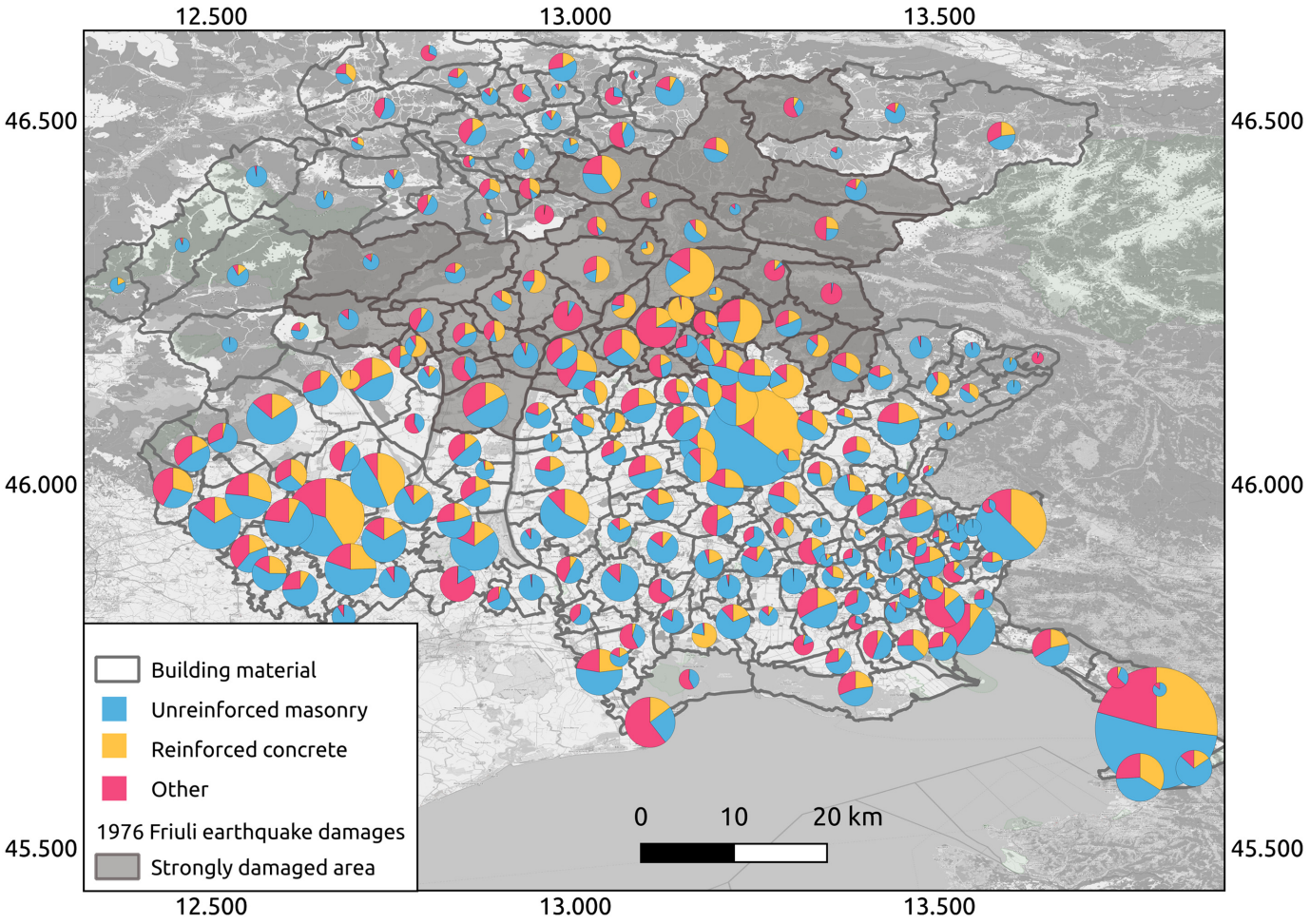

Figure 2. Spatial distribution of building materials for the FVG region. Pie charts show, for each municipality, the proportion of buildings for each building material class identified in the Italian National Institute of Statistics (ISTAT) (2011) census. The pie chart size is proportional to the number of buildings in the municipality. The area that suffered strong damages during the 1976 Friuli earthquake is highlighted with gray shading. The color version of this figure is available only in the electronic edition.

their geographic area of validity and the compatibility with the local building typologies of the FVG. The following models have been selected:

1. Ahmad *et al.* (2011): Fragility curves derived numerically for buildings typical of the Euro-Mediterranean area. Specific curves are provided for RC (ductile or nonductile, regular or irregular, low or mid or high rise) and URM (stone or fired brick with high or low percentage of voids);
2. Borzi, Crowley, and Pinho (2008) and Borzi, Pinho, and Crowley (2008): Fragility curves derived numerically for RC (seismically/nonseismically designed) and low or mid-rise URM (low or high-quality stone, brick having low or high percentage of voids). The model was originally defined for three damage levels, and it has subsequently empirically reimplemented to five levels by Faravelli *et al.* (2019), based on the observed damage data collected from seven earthquakes in Italy;
3. Karantoni *et al.* (2011): Fragility curves derived numerically for European URM buildings (2/4/6 storeys, flexible or rigid floors);
4. Rota *et al.* (2008): Empirical fragility curves derived by the damage data collected after five earthquakes in Italy. Curves are provided for low- and mid-rise buildings constituted by RC (seismically/nonseismically designed), URM (regular or irregular, flexible or rigid floors, with or without tie rods or beams), and mixed buildings.

Figure 4 presents an example of the fragility curves proposed by the four considered authors for low-rise URM buildings. All curves use PGA as ground-motion IM. There are substantial differences between the different fragility models proposed, due to the different methodologies adopted (empirical, analytical, and hybrid) and the different datasets used for their calibration. Some of the existing continuous fragility curves have a very steep ascending curve, leading to the estimation of high-damage fractions at low ground-motion intensity levels. In case of empirically derived curves, this is likely related to the statistical fitting. In fact, observed damages are usually less frequent for lower

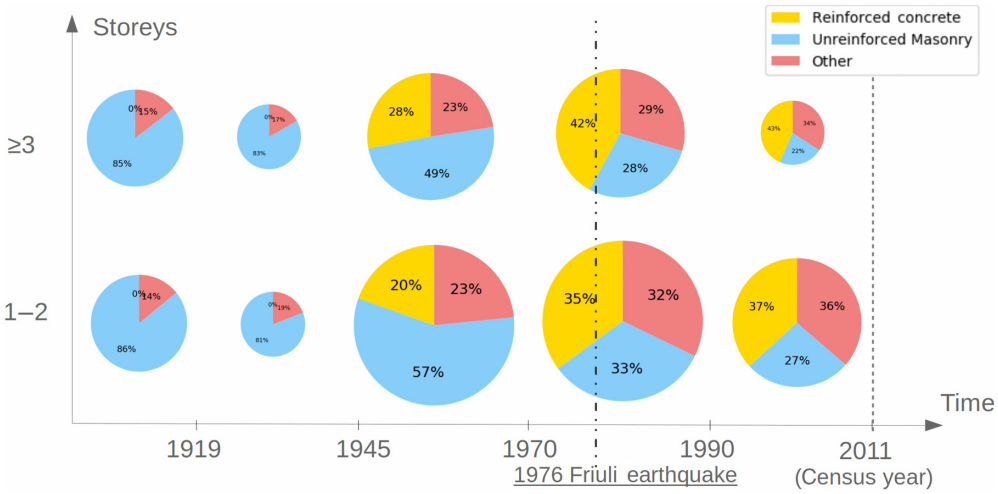

Figure 3. Temporal distribution of the building typologies identified from the ISTAT (2011) database. The pie charts show the percentage of buildings in each building material class for each time interval (*x* axis) and number of storey class (*y* axis). The pie chart size is proportional to the total number of buildings in each age and storey class. The dashed line shows the occurrence of the 1976 Friuli earthquake. For the sake of simplicity, and given the low presence of high-rise buildings, the number of storeys has been grouped into only two classes. The color version of this figure is available only in the electronic edition.

ground-motion intensity, whereas, the most damage forms are filled in the epicentral area where higher ground motion is expected. In addition, the process of assigning a damage level is prone to higher errors compared to extensive or complete damages, so the uncertainty can be higher for intermediate damage levels. The difficulties in estimating nonstructural damages based on data that are normally collected in the epicentral area is also pointed out by De Luca *et al.* (2015). Thus, fragility curves were discretized, and, a minimum PGA value of 0.2*g* was selected, to avoid the damage overestimation at low ground shaking. Because the civil protection operators are mostly interested in identifying areas where high damages (D4–D5) are expected, discarding the damage contribution at low ground motions helps fulfilling the operational aim of the tool. However, this assumption has very strong limitations and should be validated using more sophisticated approaches.

We associated each identified building typology of the exposure model to one or more fragility curves for each author (Table 1). The naming convention for the building types is extracted from the SYNER-G fragility curves archive (SYNER-G deliverable 7.1, SYNER-G, 2009), with the exception of the curves of Borzi, for which we used the vulnerability classification adopted by Faravelli *et al.* (2019). Guidelines for the development and choice of fragility functions, based on a quality rating, have been provided by Rossetto *et al.* (2013). If specific curves for a building typology were not available, we use the most compatible with the typology. If an author presents more than one curve compatible with the same typology, we based our choice on assumptions on the construction techniques used in the different time periods. For example, Rota *et al.* (2008) propose different types of brick masonry with rigid or flexible floors. We selected the typology that most reasonably matches the existing buildings in the study area. In ambiguous cases or in absence of other information, we conservatively selected the less-resistant one (e.g., flexible floors).

The following assumptions are used to associate the exposure categories with a fragility model:

1. We assume that masonry buildings constructed before 1945 are constituted by stone masonry, whereas, modern masonry is constituted by bricks and/or blocks.
2. Because many authors propose fragility curves for low-rise (1–2 storeys) and mid-rise (3–4 storeys) buildings, the exposure classes were defined accordingly.
3. Age classification is different between masonry and RC, due to their different presence over time (Fig. 3): masonry buildings typologies are more heterogeneous in the past, whereas RC typologies have been largely employed in recent decades, and underwent substantial advances in seismic design.
4. Because, it was confirmed by a number of local practitioners interviewed for this study, the "other or mixed material" category seems to be referred mostly to buildings that are constituted by a mixed vertical structure (URM and RC). Given that not all authors provide fragility curves for " other or mixed" material, under the assumption that most mixed buildings in Italy are constituted by a combination of load-bearing masonry and RC, we precautionary use fragility curves for masonry, with the exception of the curves specifically proposed by Rota *et al.* (2008) for buildings constructed with mixed techniques.
5. Rota *et al.* (2008) propose two different curves for regular URM, having respectively flexible and rigid floors. According to building inspections, analysis of building projects and interviews with municipality technicians, historical masonry in the region was normally built with wooden roofs, whereas, postwar buildings are mostly constituted by bricks or blocks or RC and have hollow tiles mixed floors. Thus, we hypothesize that historical masonry has flexible floors, whereas, modern masonry has rigid floors.

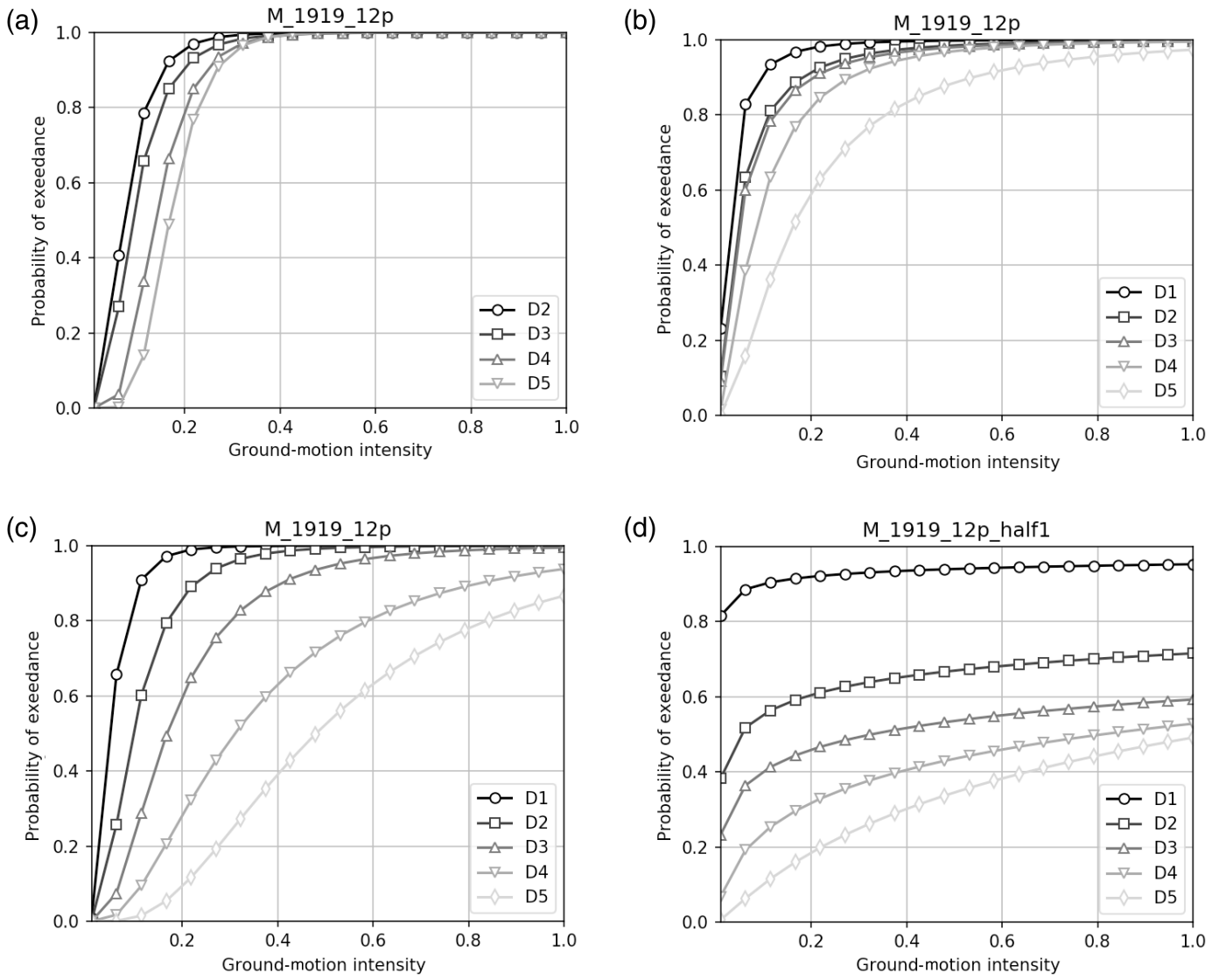

Figure 4. (a) Ahmad *et al.* (2011); (b) Borzi, Crowley, and Pinho (2008) and Borzi, Pinho, and Crowley (2008) (c) Karantoni *et al.* (2011); (d) Rota *et al.* (2008). Example of fragility curves proposed by different authors for high vulnerability or historical unreinforced masonry (URM), low rise (1–2 storeys). Damage levels (D1–D5) are defined as from the European Macroseismic Scale 1998 (EMS-98) scale. The considered ground-motion intensity is PGA for the four sets of curves.

Because Karantoni *et al.* (2011) does not provide curves for RC buildings, the RC curves are selected among the three remaining curves of Rota *et al.* (2008), Borzi, Crowley, and Pinho (2008), Borzi, Pinho, and Crowley (2008), and Ahmad *et al.* (2011).

6. After the 1976 earthquake, the strongly damaged area (highlighted in Fig. 2) underwent an extensive postevent reconstruction. To account for it, some modifications were made to the exposure data. In particular, the RC and mixed buildings constructed after 1970 were classified as seismically designed, accounting for the increased resistance of the reconstructed buildings.

The RDSA System

Computational infrastructure

To rapidly evaluate the potential damage distribution after a significant earthquake event, OGS has developed an automatic system integrated with the seismic monitoring network of the CRS and directly bonded to the head quarter of the PCR in Palmanova, which receives ground shaking and structural damage forecasts in almost real time. A schematic representation of the damage scenario calculation workflow is summarized in Figure 5.

When an event of magnitude exceeding a predefined threshold level (in this case M_L 3) is detected by the network, the CRS alert system triggers, initially, the calculation of the ground shaking scenario on a dedicated ShakeMap server. After successful completion, the RDSA process is, thus, started to compute

TABLE 1
Building Typologies Identified in the Study Area and Fragility Curves Associated to Each Typology

Building Typology			Fragility Curves		
Material	**Age**	**Storey**	**Author**	**Type**	**Description**
URM	<1920	1–2	Borzi	A	High-vulnerability masonry, low rise
			Ahmad	URM stones	URM with stones work, low rise
			Karantonin	2FT	Masonry, flexible roofs, one door at ground storey and all other openings are windows, two storey
			Rota	IMA2	Masonry, irregular layout, flexible floors, without tie rods or tie beams, 1–2 storeys
		3–4	Borzi	A	High-vulnerability masonry, medium rise
			Ahmad	URM stones	URM with stones work, mid rise
			Karantonin	4FT	Masonry, flexible roofs, one door at ground storey and all other openings are windows, four storey
			Rota	IMA6	Masonry, irregular layout, flexible floors, without tie rods or tie beams, >three storey
		>5	Borzi	A	High-vulnerability masonry, medium rise
			Ahmad	URM stones	URM with stones work, mid rise
			Karantonin	4FT	Masonry, flexible roofs, one door at ground storey and all other openings are windows, four storey
			Rota	IMA6	Masonry, irregular layout, flexible floors, without tie rods or tie beams, >three storey
	1920–1945	1–2	Borzi	A	High-vulnerability masonry, low rise
			Ahmad	URM stones	URM with stones work, low rise
			Karantonin	2FT	Masonry, flexible roofs, one door at ground storey and all other openings are windows, two storey
			Rota	RMA2	Masonry, regular layout, flexible floors, without tie rods or tie beams, 1–2 storeys
		3–4	Borzi	A	High-vulnerability masonry, medium rise
			Ahmad	URM stones	URM with stones work, mid rise
			Karantonin	4FT	Masonry, flexible roofs, one door at ground storey and all other openings are windows, four storey
			Rota	RMA6	Masonry, regular layout, flexible floors, without tie rods or tie beams, >three storey
		>5	Borzi	A	High-vulnerability masonry, medium rise
			Ahmad	URM stones	URM with stones work, mid rise
			Karantonin	4FT	Masonry, flexible roofs, one door at ground storey and all other openings are windows, four storey
			Rota	RMA6	Masonry, regular layout, flexible floors, without tie rods or tie beams, >three storey
	1946–1990	1–2	Borzi	B	Medium-vulnerability masonry, medium rise
			Ahmad	URM bricks	URM with fired brick having high percentage of voids, low rise

The typology codes adopted in the tables are the same of the SYNER-G fragility curves archive (SYNER-G, 2013). RC, reinforced concrete; URM, unreinforced masonry.
*Values for RC3 are not given by the authors; thus, RC1 curves are used.
(Continued next page.)

TABLE 1 (continued)

Building Typologies Identified in the Study Area and Fragility Curves Associated to Each Typology

Building Typology			Fragility Curves		
Material	**Age**	**Storey**	**Author**	**Type**	**Description**
			Karantonin	2RT	Masonry, rigid roofs, one door at ground storey and all other openings are windows, two storey
			Rota	RMA2	Masonry, regular layout, flexible floors, without tie rods or tie beams, 1–2 storeys
		3–4	Borzi	B	Medium-vulnerability masonry, medium rise
			Ahmad	URM bricks	URM with fired brick having high percentage of voids, mid rise
			Karantonin	4RT	Masonry, rigid roofs, one door at ground storey and all other openings are windows, four storey
			Rota	RMA6	Masonry, regular layout, flexible floors, without tie rods or tie beams, >three storey
		>5	Borzi	B	Medium-vulnerability masonry, medium rise
			Ahmad	URM bricks	URM with fired brick having high percentage of voids, mid rise
			Karantonin	4RT	Masonry, rigid roofs, one door at ground storey and all other openings are windows, four storey
			Rota	RMA6	Masonry, regular layout, flexible floors, without tie rods or tie beams, >three storey
	>1990	1–2	Borzi	C1	Low-vulnerability masonry, medium rise
			Ahmad	URM bricks	URM with fired brick having low percentage of voids, low rise
			Karantonin	2RT	Masonry, rigid roofs, one door at ground storey and all other openings are windows, two storey
			Rota	RMA4	Masonry, regular layout, rigid floors, without tie rods or tie beams, 1–2 storeys
		3–4	Borzi	C1	Low-vulnerability masonry, medium rise
			Ahmad	URM bricks	URM with fired brick having low percentage of voids, mid rise
			Karantonin	4RT	Masonry, rigid roofs, one door at ground storey and all other openings are windows, four storey
			Rota	RMA8	Masonry, regular layout, rigid floors, without tie rods or tie beams, 3 >three storey
		>5	Borzi	C1	Low-vulnerability masonry, medium rise
			Ahmad	URM bricks	URM with fired brick having low percentage of voids, mid rise
			Karantonin	4RT	Masonry, rigid roofs, one door at ground storey and all other openings are windows, four storey
			Rota	RMA8	Masonry, regular layout, rigid floors, without tie rods or tie beams, 3 >three storey
Other	All ages	1–2	Rota	MX1	Mixed, 1–2 storeys
		3–4	Rota	MX2	Mixed, >three storey
		>5	Rota	MX2	Mixed, >three storey
RC	<1970	1–2	Borzi	C2	RC nonseismically designed

The typology codes adopted in the tables are the same of the SYNER-G fragility curves archive (SYNER-G, 2013). RC, reinforced concrete; URM, unreinforced masonry.
*Values for RC3 are not given by the authors; thus, RC1 curves are used.
(Continued next page.)

TABLE 1 (continued)

Building Typologies Identified in the Study Area and Fragility Curves Associated to Each Typology

Building Typology			Fragility Curves		
Material	**Age**	**Storey**	**Author**	**Type**	**Description**
			Ahmad	RC irregular nonductile	RC nonductile frame structures, irregular, low rise, two storey
			Rota	RC2	RC, no seismic design, 1–3 storeys
		3–4	Borzi	C2	RC nonseismically designed
			Ahmad	RC irregular nonductile	RC nonductile frame structures, irregular, mid-rise, five storey
			Rota	RC4	RC, no seismic design, ≥four storey
		>5	Borzi	C2	RC nonseismically designed
			Ahmad	RC irregular nonductile	RC nonductile frame structures, irregular, high rise, eight storey
			Rota	RC4	RC, no seismic design, ≥four storey
	1970–1990	1–2	Borzi	C2	RC nonseismically designed
			Ahmad	RC regular nonductile	RC nonductile frame structures, regular, low rise, two storey
			Rota	RC2	RC, no seismic design, 1–3 storeys
		3–4	Borzi	C2	RC nonseismically designed
			Ahmad	RC regular nonductile	RC nonductile frame structures, regular, medium rise, five storey
			Rota	RC4	RC, no seismic design, ≥four storey
		>5	Borzi	C2	RC nonseismically designed
			Ahmad	RC regular nonductile	RC nonductile frame structures, regular, high rise, eight storey
			Rota	RC4	RC, no seismic design, ≥four storey
	1990–2005	1–2	Borzi	D	RC seismically designed
			Ahmad	RC regular nonductile	RC nonductile frame structures, regular, low rise, two storey
			Rota	RC2	RC, no seismic design, 1–3 storeys
		3–4	Borzi	D	RC seismically designed
			Ahmad	RC regular nonductile	RC nonductile frame structures, regular, medium rise, five storey
			Rota	RC4	RC, no seismic design, ≥four storey
		>5	Borzi	D	RC seismically designed
			Ahmad	RC regular nonductile	RC nonductile frame structures, regular, high rise, eight storey
			Rota	RC4	RC, no seismic design, ≥four storey
	>2005	1–2	Borzi	D	RC seismically designed
			Ahmad	RC regular ductile	RC ductile frame structures, regular, low rise, two storey
			Rota	RC1	RC, seismic design, 1–3 storeys
		3–4	Borzi	D	RC seismically designed
			Ahmad	RC regular ductile	RC ductile frame structures, regular, medium rise, five storey
			Rota	RC1*	RC, seismic design, 1–3 storeys
		>5	Borzi	D	RC seismically designed
			Ahmad	RC regular ductile	RC ductile frame structures, regular, high rise, eight storey
			Rota	RC1*	RC, seismic design, 1–3 storeys

The typology codes adopted in the tables are the same of the SYNER-G fragility curves archive (SYNER-G, 2013). RC, reinforced concrete; URM, unreinforced masonry.
*Values for RC3 are not given by the authors; thus, RC1 curves are used.

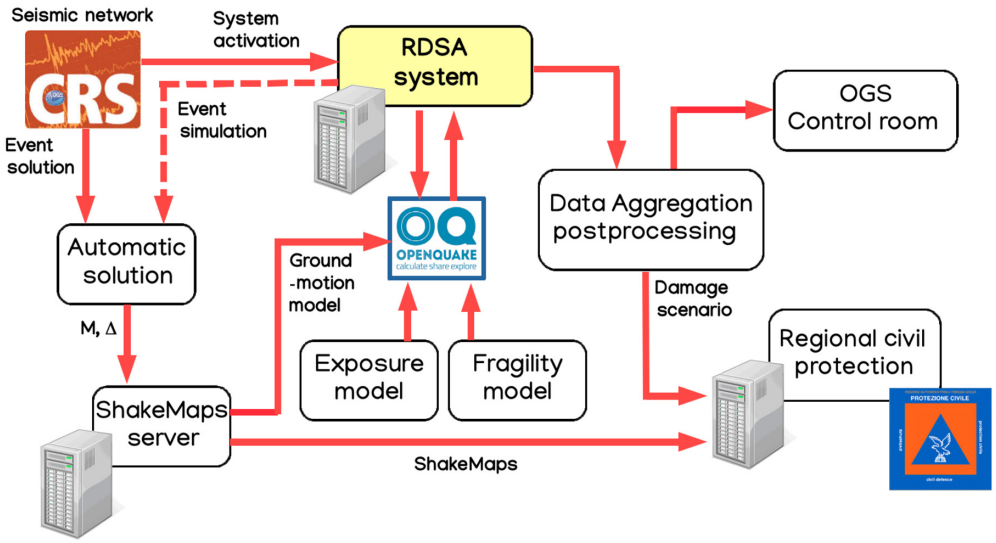

Figure 5. Schematic representation of the calculation workflow of the rapid damage scenario assessment (RDSA) system. OGS, National Institute of Oceanography and Applied Geophysics. The color version of this figure is available only in the electronic edition.

the damage distribution associated to the event. The actual damage calculation is performed in background by the OQ software engine, an open-source software written in the Python programming language for earthquake hazard and risk analysis (Pagani *et al.*, 2014). The software receives and converts the input ground-shaking model from the ShakeMap server and combines it with exposure information, aggregated at municipality level, and the selected fragility models. It must be noted that, to produce a more statistically consistent evaluation of the expected damage, the uncertainty associated with the input empirical ground-motion model is sampled by the OQ calculation engine, to produce a spectrum of damage scenarios, which are averaged in output. A number of 100 random samples is used in each calculation. Moreover, we are currently working on including ground-motion correlation models, to better depict the spatial variability of the ground motion.

Calculation results are then postprocessed by aggregating building typologies and damage levels (severe damage to total collapse, D4 + D5 of the EMS-98 scale). The associated number of people potentially impacted is also computed, based on the simplified empirical relationship developed for the IRMA, as described in Dolce *et al.* (2019). The whole scenario information is, thus, packed in geoJSON format and finally delivered to the database of the PCR, using a protected communication channel.

Interfacing the PCR

Each computed scenario is archived both internally in the RDSA system and into the local database of the PCR, ready to be visualized in the emergency control room by mean of an ad hoc WebGIS interface, developed to support emergency operators in the postevent intervention process.

The visualization interface of the PCR is specifically designed to highlight only the most essential information required by the emergency operators (Fig. 6). Together with the basic earthquake parameters (magnitude, local time, epicentral location, and depth), ground shaking and damage distributions (aggregated at municipality level) are presented simultaneously, but on separate maps, to facilitate a quick evaluation of the affected area, while allowing at the same time a clear separation between regions of perception and those affected by potential damage. For quick reference, the list of municipalities with larger estimated number of damaged buildings and the associated casualties predicted empirically is also provided.

Simulated scenarios

It must be mentioned that, complementary to the real-time purpose of the application, the RDSA system allows for offline calculation of user-defined testing scenarios, for the use in specialized training and capacity-building activities, and in support of mid-to-long-term prevention strategy planning. As for actual events, the testing scenarios calculated by OGS are also delivered to the PCR for local archiving, with the goal of creating a database of simulated scenarios chosen as most representative of the regional earthquake hazard.

In case of simulated earthquake events, the RDSA system triggers a virtual calculation on the ShakeMap server. In this case, the simulation differs from a real event in that the input ground-motion scenario is not constrained by any actual recording, but only empirically estimated based on the desired size and location of the target event. To avoid misinterpretation of the simulated alarm, then, such calculation is marked with a special identification code, which is then recognized by the civil protection and, thus, properly flagged as simulation. This functionality is essential for the testing and verification of the system, but it is also suitable for routine training activities of the operators and emergency planning.

Considerations on latency

A damage scenario is usually available from the RDSA system, within less than 4 min from the issuing of the earthquake alert. The latency of the calculation chain, however, is controlled differently by the various steps involved in the process. The

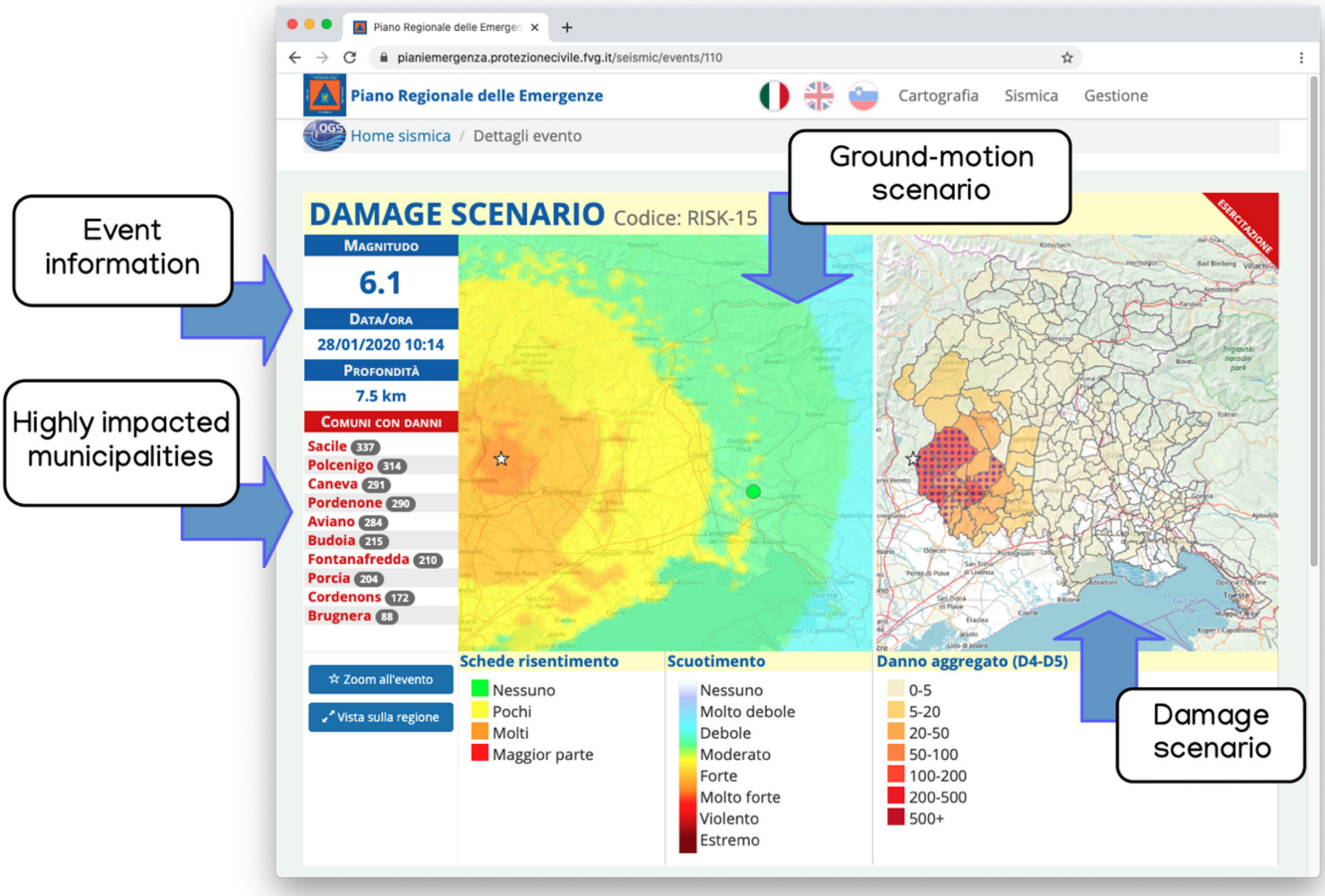

response delay of the network alert system is variable and depends on the distance of the earthquake to the closest stations of the network, with some overhead related to data collection and preprocessing. On average, an alert time of 1–2 min can be considered a reasonable upper bound, for events occurring within a buffer of 50 km around the FVG region.

Neglecting the minimal delay introduced by communication between machines, the largest latency is, therefore, due to the calculation of the ground motion and damage scenarios. The actual damage scenario calculation requires about 30 s on our machine, to perform with the current exposure model configuration. The ShakeMap server, however, introduces a longer delay (about 180 s) due to the need of collecting sufficiently long signal windows for the calculation of the ground-motion parameters required to constrain the ground-shaking scenario. Such delay cannot be substantially decreased. A possible workaround could consist in delivering a preliminary damage model initially not conditioned by observed ground motion, and, subsequently, update the model when new information is progressively available. It is to mention, however, that, for operative purposes, a total delay time of up to 5 min appears, nonetheless, acceptable, therefore, further optimizations are presently unnecessary.

Figure 6. Screenshot of the Web-GIS interface of the Civil Protection of the FVG region. The graphical interface is designed to be used by emergency operators in the control room, and it allows a rapid visualization of the most essential earthquake information and the associated ground motion and damage scenarios. The color version of this figure is available only in the electronic edition.

Testing and Validation

The target scenario

The RDSA system has been tested against the damage information collected after the M_L 6.4 Friuli earthquake of May 1976, considered one of the most devastating earthquakes in Italy of the last century. The event killed about 1000 people and destroyed more than 18,000 houses (plus 70,000 heavily damaged), leaving over 100,000 people homeless. Following the event, around 85,000 damage reports (Riuscetti *et al.*, 1997; Carniel *et al.*, 2001; Grimaz, 2009; Grimaz and Malisan, 2018) have been thoroughly collected, for the purpose of supporting the financial allocation and distribution of the reconstruction budget. Nowadays, such material represents an important source of information for a variety of earthquake engineering

studies, including calibration of fragility and economical loss models.

In this study, we used these damage reports to infer the number of damaged buildings in the epicentral area (45 municipalities classified as destroyed by the regional law after the event). Because of some potential bias related to the political situation (Riuscetti *et al.*, 1997), we limited our analysis to the high-damage levels, corresponding to the D4–D5 level of the EMS-98 classification. Among different proposed relations, to convert from the reported information to EMS-98 damage levels, we adopted the one proposed by Faravelli *et al.* (2019). It must be noted that after the 1976 event, not all collapsed buildings were associated to a damage report (Carniel *et al.*, 2001). Thus, it was necessary to complement the missing information with regional statistics performed at municipality level in 1986 (Floriana Marino, personal comm., 2019), containing the number of fully reconstructed buildings in the epicentral area. For each municipality, then, we subtracted the number of destroyed buildings according to the 1976 damage forms and estimated the number of collapsed buildings. Given that the regional statistics were done in 1986 (when the reconstruction was almost completed) and that most villages were extensively reconstructed, this simplified approach should provide more realistic results.

Exposure and fragility model adjustment

To model exposure, accordingly, at the time of this scenario, we used a modified version of the Italian National Institute of Statistics (ISTAT) (2011) census database, for which all buildings constructed after 1976 have been discarded (roughly halving the number of buildings for the 1970–1980 decade and removing those ones after 1980). In addition, to account for the effect of reconstruction in the epicentral area, and knowing that before 1976 masonry was the most common building typology in the area, we have converted the remaining RC and mixed buildings dated before 1990 into URM. The choice was taken based on the examination of the post-1976 damage forms (Carniel *et al.*, 2001) and reconstruction projects (Gentilli and Croatto, 2008), and the archive of the TiereMotus museum, dedicated to the post-1976 reconstruction (Venzone, Udine).

Assuming that the modeled exposure and damage information is consistent with observations, we have also investigated the role of the selected fragility models on the damage distribution. We performed four different runs of the model, initialized with the same ground motion and exposure data but with four different fragility curves groups. Then, we compared the resulting heavy damages (D4–D5 of the EMS-98 scale) with the post-1976 damage forms, converted into EMS-98 damage levels using the method proposed by Faravelli *et al.* (2019). Results show that the two sets of fragility curves that better fit the damage data in the epicentral area are Borzi and Ahmad (Fig. 7), which better reproduce the damages occurred in the epicentral area in 1976. In particular, we observed that these curves are particularly suitable for historical masonry, widely distributed in the region before 1976. We also observed that the curves of Rota and Karantoni better reproduce the damages reported by municipalities far from the epicenter. However, reports from less damaged areas were often incomplete, not exhaustive or less accurate than those collected for the epicentral area (Carniel *et al.*, 2001; Grimaz and Malisan, 2018).

Because of the high differences in today's building stock (retrofitted and/or enriched with modern building typologies), the substantial differences in the four selected fragility curve groups and the high uncertainty in their selection for specific typologies, we decided to combine the use of the four curves within a logic-tree structure. The damage is thus calculated by redistributing the number of buildings of each typology between the four fragility curve branches, scaled proportionally to a specific weighting schema that reflects the confidence on each fragility model. Because of the lack of calibration data, however, weights are, presently, equally distributed between branches, but it is our strategy to allow ad hoc weighting whenever new information becomes progressively available. Adopting a logic-tree approach is allowing to account for the epistemic uncertainty affecting the selection of the fragility curves also at operational level. We are, nonetheless, performing further analyses, to calibrate the model and account for both epistemic and aleatory uncertainty.

Results and discussion

We assess the expected damage for the May 1976 ground-motion scenario under two different conditions:

1. Pre-1976: The exposure dataset is the one used for the calibration process, modified from the ISTAT (2011) census as described in precedence. We use the fragility curves proposed by Borzi, Crowley, and Pinho (2008), Borzi, Pinho, and Crowley (2008), and Ahmad *et al.* (2011), which showed to better reproduce the documented damages after the 1976 event (Fig. 7). We, therefore, run the model using the two sets of fragility curves, combined with equal weights. Because Ahmad *et al.* (2011) do not propose fragility curves for RC, only the curves proposed by Borzi, Crowley, and Pinho (2008) and Borzi, Pinho, and Crowley (2008) were used for RC buildings.
2. Post-1976: We run the model using a fragility model, based on the tree-structure combination of the four selected fragility curves, all with equal weights. Because Ahmad *et al.* (2011) do not propose fragility curves for RC, the other three curves were combined with equal weights for buildings in that typology.

Results of the damage assessment estimation for the pre-1976 and post-1976 conditions are shown in Figure 8. The maps show that the percentage of damaged buildings, due to an

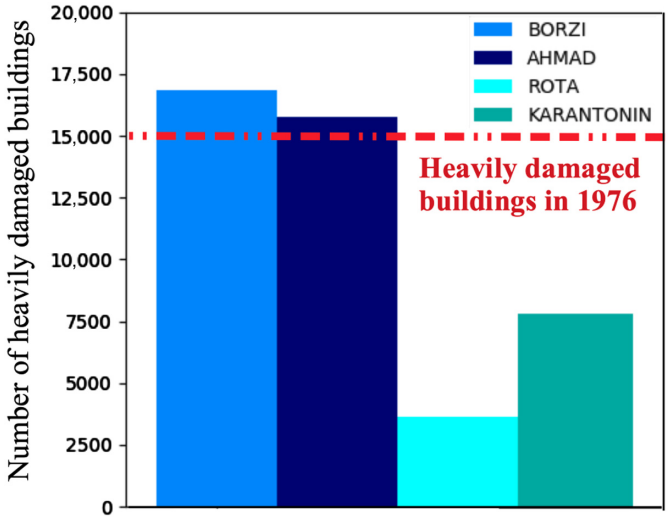

Figure 7. Number of heavily damaged buildings estimated for the epicentral area. The calculation was run using the four fragility curves selected (see legend). The dashed line shows the number of heavily damaged buildings, according to the postevent damage assessment. The color version of this figure is available only in the electronic edition.

event similar to the May 1976 earthquake with the current exposure, is substantially lower. It is worth noticing that, with respect to the pre-1976 simulation, in the post-1976 scenario the total aggregated damage is characterized by a large fraction of building in damage state D4.

In particular, approximately, 12,000 and 11,000 buildings in the region are expected to suffer strong damages (D4 + D5), for the pre-1976 and post-1976 simulation, accounting, respectively, for the 5% and 4% of the total building stock in the region. However, the absolute number of buildings expected to suffer damage of any level (D1–D5) increases from 16,000 to 22,000, from pre-1976 to post-1976 conditions, accounting for the 7% of total buildings in both cases. The discrepancy between percentages and absolute number of damaged buildings are due to the different exposure models used: the post-1976 exposure model contains, approximately, 90,000 additional buildings, mostly constructed during the strong Italian economic expansion (Pietroforte and Tangerini, 2000) and, thus, not compliant with the recent building regulations.

From the results of this analysis, it is now clear that a full validation exercise, based on the 1976 Friuli earthquake, cannot be unambiguously performed, because of the limitations in reproducing the 1976 conditions. In facts, the main limitations we are facing are (1) the lack of recordings during the 1976 event, which limits our ability to reproduce a realistic scenario, (2) the not complete reliability of data collected during the 1976 Friuli earthquake, when compared to recent damage forms, and (3) the difficulty in reproducing the exposure conditions of the time due to the lack of census data. Nonetheless, these preliminary results have shown, at least, qualitatively that, despite the strong reconstruction effort that followed the 1976 event, the damages expected in case of similar scenarios could still be substantial. We argue that the positive effect of building stock retrofitting might be, nowadays, effectively counterbalanced by the increased number of buildings (and, thus, an increase of the exposed assets), keeping in mind that the predicted damage could also be overestimated by the use of not-properly calibrated fragility models.

Outlook and Conclusions

We developed a system for rapid evaluation of the expected damage distribution caused by a significant earthquake event, aimed at supporting emergency intervention activities of the PCR. The system closely integrates with the seismological network of the CRS, from which it receives earthquake alerts with event information in almost real time. Along with the operational application, the RDSA system has been conceived as a testing platform for the progressive development and validation of new seismological and engineering methodologies. In fact, the tool is presently under active development, and several important features are scheduled for future releases.

As a starting point, it is our plan to reduce the uncertainty of the damage prediction by better depicting the variety and distribution of the main building typologies in the region, for example, improving the exposure model by including more realistic classification proxies, such as elevation and aspect ratio, and by increasing the resolution scale of our analysis from municipality to districts or quarters. As well, we aim at improving the current fragility model by implementing ad hoc damage functions for the most common building typologies of the FVG region. Unfortunately, there are still open issues to be tackled, to assess the expected dynamic behavior of building. In particular, the contribution of different ground-motion parameters other than the PGA is required to realistically assess the expected damage (Masi *et al.*, 2011; Chiauzzi *et al.*, 2012; Gehl *et al.*, 2013). Furthermore, uncertainty associated to fragility models (Bradley, 2010) and the subsequent effect on damage assessment results needs to be accounted in a more systematic manner.

As a major limitation, the system does not presently account for cumulative damage during an earthquake sequence. So far, just the damage corresponding to the largest event is considered, which is necessary but an unrealistic simplification. For instance, four months after the Friuli 1976 mainshock, four seismic events of M_w ranging from 5.3 to 6 stroke again the same area and caused substantial damages to buildings, in particular, those previously damaged. Although, a strategy for the progressive update of the exposure model is currently under development, the implementation of a time-dependent damage model is more challenging (e.g., Iervolino *et al.*, 2016, 2020), because it requires calibration information not readily available. Further work is, thus,

Figure 8. Results of two damage scenarios, based on the May 1976 seismic event, for two different conditions: (a–c) pre-1976 and (d–f) post-1976. The percentage of buildings in each damage level (D4 + D5, D5, and D4) is shown in the first, second, and third column, respectively. The color version of this figure is available only in the electronic edition.

required to support emergency managers, during the whole seismic sequence, and ad hoc studies are presently ongoing on the matter.

Although, the improvement of the structural component is necessary to improve the prediction accuracy, a better depiction of the underlying ground-motion hazard is equally paramount. The ground-motion model currently used is affected by a large uncertainty, particularly, on the site term. For future releases of the tool, it is our intention to use more sophisticated ground-motion models, calibrated on local data available from the seismological networks and from a number of seismic response characterization analysis we are conducting on the territory.

Being the tool strongly oriented to practical operative purposes, it is of uppermost significance for us to receive and integrate the feedback from end users of our products and stakeholders. Because of that, the WebGIS visualization tool has been developed in collaboration with the PCR of the FVG, following the recommendation of the control room emergency operator, whose focus is on practical and direct usability of the product. We are currently working on extending the target area to include the Veneto region, in strict collaboration with the local PCR, and, a preliminary version of the tool has been implemented, following the recommendations of the Accelerometric Real-time Monitoring Network for sites and buildings in Italy and Austria project (project ID ITAT3016). As well, we envisage the cross-border cooperation with our neighboring countries (Austria and Slovenia) for the development of harmonized procedures for real-time damage assessment.

We are confident that the current research will contribute in increasing preparedness and response capacity, in case of damaging events, for example, by continuous integration of the feedback from civil protection, binding the target of our research to practical usability, such as the support for training activities and long-term territorial planning.

Data and Resources

The data used to generate the ShakeMap were collected by the following seismic networks. The northeast Italy seismic network (OX, doi: 10.7914/SN/OX). The northeast Italy broadband network (NI, doi: 10.7914/SN/NI). The Trentino seismic network (ST, doi: 10.7914/SN/ST). The Collalto seismic network (EV, doi: 10.7914/SN/EV). The Friuli Venezia Giulia (FVG) accelerometric network (RF, doi: 10.7914/SN/RF). The Italian seismic network (IV, doi: 10.13127/SD/X0FXnH7QfY). The Italian strong-motion network (IT, doi: 10.7914/SN/IT). The seismic network of the Republic of Slovenia (SL, doi:

10.7914/SN/SL). The Austrian seismic network (OE, doi: 10.7914/SN/OE). The ShakeMap is a software released by the U.S. Geological Survey (USGS; https://usgs.github.io/shakemap/index.html), whereas, the Italian configuration was provided by Alberto Michelini e Licia Faenza (Istituto Nazionale di Geofisica e Vulcanologia [INGV]). Some maps were produced using the open-source QGIS Geographic Information System (http://qgis.org). The OpenQuake (OQ) platform is available at https://platform.openquake.org/vulnerability/list. All websites were last accessed in October 2020.

Acknowledgments

The authors are grateful to the technical staff of the National Institute of Oceanography and Applied Geophysics (OGS) Centro di Ricerche Sismologiche (CRS) for their efforts in the management with the information technology infrastructures and in the maintenance of the stations. The "Rete Sismometrica del Friuli Venezia Giulia" is managed by OGS with the financial contribution of the Regione Autonoma Friuli Venezia Giulia (FVG). The "Rete Sismometrica del Veneto" is managed by OGS with the financial contribution of the Regione Veneto. This research was partially funded by the Civil Protection of FVG and Veneto. The authors thank the Civil Protection staff, in particular, Aldo Primiero for the useful discussions and Stefano Salvador for the technical support. A special thank goes to Floriana Marino (Museo Tiere Motus Venzone) for providing information about the damaged buildings after the Friuli 1976 earthquake. The authors are grateful to the reviewers Carmine Galasso and Ricardo Monteiro for their time in reviewing this article and for the many insightful suggestions, which were essential to improve the article, clarify some aspects of our research, and trigger new ideas for future developments. We also thank the Istat national offices (Rome) and the regional office of Friuli Venezia Giulia for providing the census data at census unit scale.

References

Ahmad, N., H. Crowley, and R. Pinho (2011). Analytical fragility functions for reinforced concrete and masonry buildings and buildings aggregates of Euro-Mediterranean regions—UPAV methodology, *Intern. Rep., Syner-G Project 2009/2012*.

Bal, I. E., J. J. Bommer, P. J. Stafford, H. Crowley, and R. Pinho (2010). The influence of geographical resolution of urban exposure data in an earthquake loss model for Istanbul, *Earthq. Spectra* **26,** no. 3, 619–634, doi: 10.1193/1.3459127.

Bal, I. E., H. Crowley, and R. Pinho (2008). Displacement-based earthquake loss assessment for an earthquake scenario in Istanbul, *J. Earthq. Eng.* **12,** sup2, 12–22, doi: 10.1080/13632460802013388.

Bommer, J. J. (2002). Deterministic vs. probabilistic seismic hazard assessment: An exaggerated and obstructive dichotomy, *J. Earthq. Eng.* **6,** 43–73.

Borzi, B., H. Crowley, and R. Pinho (2008). Simplified pushover-based earthquake loss assessment (SP-BELA) method for masonry buildings, *Int. J. Archit. Herit.* **2,** no. 4, 353–376.

Borzi, B., M. Faravelli, and D. A. Polli (2019). Central Italy sequence: Simulated damage scenario for the main 2016 shocks, *Bull. Earthq. Eng.* **17,** 5559–5581, doi: 10.1007/s10518-018-0378-9.

Borzi, B., M. Onida, M. Faravelli, D. Polli, M. Pagano, D. Quaroni, A. E. CantoniSperanza, and C. Moroni (2020). IRMA platform for the calculation of damages and risks of Italian residential buildings, *Bull. Earthq. Eng.* doi: 10.1007/s10518-020-00924-x.

Borzi, B., R. Pinho, and H. Crowley (2008). Simplified pushover-based analysis for large-scale assessment of RC buildings, *Eng. Struct.* **30,** 804–820.

Bradley, B. A. (2010). Epistemic uncertainties in component fragility functions, *Earthq. Spectra* **26,** no. 1, 41–62.

Bragato, P., and A. Govoni (2000). The Friuli automatic earthquake alert system, *Boll. Geof. Teor. Appl.* **41,** no. 1, 69–77.

Bragato, P. L. (2009). Assessing regional and site-dependent variability of ground motions for ShakeMap implementation in Italy, *Bull. Seismol. Soc. Am.* **99,** no. 5, 2950–2960, doi: 10.1785/0120090020.

Bragato, P. L., P. Di Bartolomeo, D. Pesaresi, M. P. P. Linares, and A. Saraò (2011). Acquiring, archiving, analyzing and exchanging seismic data in real time at the seismological research center of the OGS in Italy, *Ann. Geophys.* **54,** 67–75, doi: 10.4401/ag-4958.

Bressan, G., P. L. Bragato, and C. Venturini (2003). Stress and strain tensors based on focal mechanisms in the seismotectonic framework of the Friuli Venezia Giulia region (Northeastern Italy), *Bull. Seismol. Soc. Am.* **93,** no. 3, 1280–1297, doi: 10.1785/0120020058.

Bressan, G., M. Ponton, G. Rossi, and S. Urban (2016). Spatial organization of seismicity and fracture pattern in NE Italy and W Slovenia, *J. Seismol.* **20,** 511–534, doi: 10.1007/s10950-015-9541-9.

Carniel, R., C. Cecotti, A. Chiarandini, S. Grimaz, E. Picco, and M. Riuscetti (2001). A definition of seismic vulnerability on a regional scale: The structural typology as a significant parameter, *Boll. Geof. Teor. Appl.* **42,** nos. 1/2, 139–157.

Chiauzzi, L., A. Masi, M. Mucciarelli, M. Vona, F. Pacor, G. Cultrera, F. Gallovič, and A. Emolo (2012). Building damage scenarios based on exploitation of Housner intensity derived from finite faults ground motion simulations, *Bull. Earthq. Eng.* **10,** 517–545, doi: 10.1007/s10518-011-9309-8.

Ciano, M., M. Gioffrè, and M. Grigoriu (2020). The role of intensity measures on the accuracy of seismic fragilities, *Probabilist. Eng. Mech.* **60,** 103041, doi: 10.1016/j.probengmech.2020.103041.

Cimellaro, G. P., G. Scura, C. S. Renschler, A. M. Reinhorn, and H. U. Kim (2014). Rapid building damage assessment system using mobile phone technology, *Earthq. Eng. Eng. Vib.* **13,** 519–533, doi: 10.1007/s11803-014-0259-4.

Cornell, C. A. (1968). Engineering seismic risk analysis, *Bull. Seismol. Soc. Am.* **58,** 1583–1606.

Crowley, H., R. Pinho, and J. J. Bommer (2004). A probabilistic displacement-based vulnerability assessment procedure for earthquake loss estimation, *Bull. Earthq. Eng.* **2,** no. 2, 173–219.

Del Gaudio, C., G. De Martino, M. Di Ludovico, G. Manfredi, A. Prota, P. Ricci, and G. M. Verderame (2017). Empirical fragility curves from damage data on RC buildings after the 2009 L'Aquila earthquake, *Bull. Earthq. Eng.* **15,** 1425–1450, doi: 10.1007/s10518-016-0026-1.

Dell'Acqua, F., P. Gamba, and K. Jaiswal (2013). Spatial aspects of building and population exposure data and their implications for global earthquake exposure modelling, *Nat. Hazards* **68,** 1291–1309, doi: 10.1007/s11069-012-0241-2.

De Luca, F., G. M. Verderame, and G. Manfredi (2015). Analytical versus observational fragilities: The case of Pettino (L'Aquila) damage data database, *Bull. Earthq. Eng.* **13,** 1161–1181, doi: 10.1007/s10518-014-9658-1.

Dolce, M., B. Borzi, F. da Porto, M. Faravelli, S. Lagomarsino, G. Magenes, C. Moroni, A. Penna, A. Prota, E. Speranza, *et al.* (2019). Seismic risk maps for the Italian territory, *XVIII ANIDIS Conf.*, Ascoli Piceno, Italy, 15–19 September 2019.

Dolce, M., and A. Goretti (2015). Building damage assessment after the 2009 Abruzzi earthquake, *Bull. Earthq. Eng.* **13,** 2241–2264, doi: 10.1007/s10518-015-9723-4.

Donà, M., P. Carpanese, V. Follador, L. Sbrogiò, and F. Da Porto (2020). Mechanics-based fragility curves for Italian residential URM buildings, *Bull. Earthq. Eng.* doi: 10.1007/s10518-020-00928-7.

Erdik, M., N. Aydinoglu, Y. Fahjan, K. Sesetyan, M. Demircioglu, B. Siyahi, E. Durukal, C. Ozbey, Y. Biro, H. Akman, *et al.* (2003). Earthquake risk assessment for Istanbul metropolitan area, *Earthq. Eng. Eng. Vib.* **2,** 1–23, doi: 10.1007/BF02857534.

Faenza, L., and A. Michelini (2010). Regression analysis of MCS intensity and ground motion parameters in Italy and its application in ShakeMap, *Geophys. J. Int.* **180,** 1138–1152, doi: 10.1111/j.1365-246X.2009.04467.x.

Faenza, L., and A. Michelini (2011). Regression analysis of MCS intensity and ground motion spectral accelerations (SAs) in Italy, *Geophys. J. Int.* **186,** 1415–1430, doi: 10.1111/j.1365-246X.2011.05125.x.

Faravelli, M., B. Borzi, D. Polli, and M. Pagano (2019). Calibration of a mechanics-based method for large-scale vulnerability assessment, *Bull. Earthq. Eng.* **17,** 2485–2508, doi: 10.1007/s10518-019-00560-0.

Gehl, P., D. M. Seyedi, and J. Douglas (2013). Vector-valued fragility functions for seismic risk evaluation, *Bull. Earthq. Eng.* **11,** 365–384, doi: 10.1007/s10518-012-9402-7.

Gentilli, R., and G. Croatto (2008). *Ilpatrimoniosalvato. Ilrecuperodell'architettura spontanea friulana dopoglieventisismici del 1976*, Forum Ed., Udine, Italy, ISBN: 978-88-8420-484-4, 448 pp.

Goretti, A., and G. Di Pasquale (2004). Building inspection and damage data for the 2002 Molise, Italy, earthquake, *Earthq. Spectra* **20,** 1_suppl, 167–190, doi: 10.1193/1.1769373.

Grimaz, S. (2009). Seismic damage curves of masonry buildings from Probit analysis on the data of the 1976 Friuli earthquake (NE Italy), *Boll. Geofis. Teor. Appl.* **50,** no. 3, 289–304.

Grimaz, S., and P. Malisan (2018). Advancements from a posteriori studies on the damage to buildings caused by the 1976 Friuli earthquake (north-eastern Italy), *Boll. Geofis. Teor. Appl.* **59,** no. 4, 505–526, doi: 10.4430/bgta0220.

Grünthal, G. (Editor) (1998). *European Macroseismic Scale 1998 (EMS-98)*, Vol. 15, European Seismological Commission, subcommission on Engineering Seismology, working Group Macroseismic Scales, Conseil de l'Europe, Cahiers du Centre Européen de Géodynamique et de Séismologie, Luxembourg.

HAZUS (1999). *Earthquake Loss Estimation Methodology—Technical And User Manuals*, Federal Emergency Management Agency, Washington, D.C.

Iervolino, I., E. Chioccarelli, and A. Suzuki (2020). Seismic damage accumulation in multiple mainshock-aftershock sequences, *Earthq. Eng. Struct. Dynam.* **49,** 1007–1027, doi: 10.1002/eqe.3275.

Iervolino, I., M. Giorgio, and E. Chioccarelli (2016). Markovian modeling of seismic damage accumulation, *Earthq. Eng. Struct. Dynam.* **45,** no. 3, 441–461, doi: 10.1002/eqe.2668.

Italian National Institute of Statistics (ISTAT) (2011). National buildings census, available at https://www.istat.it/it/censimenti-permanenti/censimenti-precedenti/popolazione-e-abitazioni/popolazione-2011 (last accessed January 2021).

Karantoni, T., F. Lyrantzaki, G. Tsionis, and M. N. Fardis (2011). Analytical fragility functions for masonry buildings and building aggregates—UPAT methodology, *Intern. Rep. Syner-G Project 2009/2012.*

Kramer, S. L. (1996). *Geotechnical Earthquake Engineering*, Prentice Hall, Upper Saddle River, New Jersey.

Masi, A., L. Chiauzzi, G. Santarsiero, V. Manfredi, S. Biondi, E. Spacone, C. Del Gaudio, P. Ricci, G. Manfredi, and G. M. Verderame (2019). Seismic response of RC buildings during the Mw 6.0 August 24, 2016 Central Italy earthquake: The Amatrice case study, *Bull. Earthq. Eng.* **17,** 5631–5654, doi: 10.1007/s10518-017-0277-5.

Masi, A., M. Vona, and M. Mucciarelli (2011). Selection of natural and synthetic accelerograms for seismic vulnerability studies on RC frames, *J. Struct. Eng.* ASCE Special Issue devoted to "Earthquake Ground Motion Selection and Modification for Nonlinear Dynamic Analysis of Structures," **137,** no. 3, 367–378.

Massa, M., P. Morasca, L. Moratto, S. Marzorati, D. Spallarossa, and G. Costa (2008). Empirical ground motion prediction equations for northern Italy using weak and strong motion amplitudes, frequency content and duration parameters, *Bull. Seismol. Soc. Am.* **98,** 1319–1342, doi: 10.1785/0120070164.

Michelini, A., L. Faenza, G. Lanzano, V. Lauciani, D. Jozinovic, R. Puglia, and L. Luzi (2020). The new ShakeMap in Italy: Progress and advances in the last 10 yr, *Seismol. Res. Lett.* **91,** 317–333, doi: 10.1785/0220190130.

Milosevic, J., S. Cattari, and R. Bento (2020). Definition of fragility curves through nonlinear static analyses: Procedure and application to a mixed masonry-RC building stock, *Bull. Earthq. Eng.* **18,** 513–545, doi: 10.1007/s10518-019-00694-1.

Moratto, L., G. Costa, and P. Suhadolc (2009). Real-time generation of ShakeMaps in the South-Eastern Alps, *Bull. Seismol. Soc. Am.* **99,** 2489–2501, doi: 10.1785/0120080283.

Moratto, L., and D. Sandron (2015). Optimizing the automatic location of the real-time Antelope system in north-eastern Italy, *Boll. Geofis. Teor. Appl.* **56,** 407–424, doi: 10.4430/bgta0154.

Moratto, L., P. Suhadolc, and G. Costa (2011). ShakeMaps for three relevant earthquakes in the Southeastern Alps: Comparison between instrumental and observed intensities, *Tectonophysics* **509,** 93–106, doi: 10.1016/j.tecto.2011.06.004.

Mouroux, P., and B. LeBrun (2006). Presentation of RISK-UE project, *Bull. Earthq. Eng.* **4,** 323–339, doi: 10.1007/s10518-006-9020-3.

Pagani, M., D. Monelli, G. Weatherill, L. Danciu, H. Crowley, V. Silva, P. Henshaw, L. Butler, M. Nastasi, L. Panzeri, *et al.* (2014). OpenQuakeEngine: An open hazard (and risk) software for the global earthquake model, *Seismol. Res. Lett.* **85,** no. 3, 692–702, doi: 10.1785/0220130087.

Palanci, M., and S. M. Senel (2019). Correlation of earthquake intensity measures and spectral displacement demands in building type structures (2019), *Soil Dynam. Earthq. Eng.* **121,** 306–326, doi: 10.1016/j.soildyn.2019.03.023.

Pietroforte, R., and P. Tangerini (2000). Regional development and construction in Italy: An input-output analysis, 1959-1992, *Construct. Manag. Econ.* **18,** no. 2, 151–159.

Priolo, E., C. Barnaba, P. G. B. Bernardis, P. L. Bragato, G. Bressan, M. Candido, E. Cazzador, P. Di Bartolomeo, G. Durì, S. Gentili, *et al.*

(2005). Seismic monitoring in northeastern Italy: A ten-year experience, *Seismol. Res. Lett.* **76,** 446–454, doi: 10.1785/gssrl.76.4.446.

Riuscetti, M., R. Carniel, and C. Cecotti (1997). Seismic vulnerability assessment of masonry buildings in a region of moderate seismicity, *Ann. Geofisc.* **40,** 1405–1413.

Rossetto, T., I. Ioannou, and D. N. Grant (2013). Existing empirical fragility and vulnerability functions: Compendium and guide for selection, *GEM Tech. Rept. 2013–X*, GEM Foundation, Pavia, Italy.

Rosti, A., M. Rota, and A. Penna (2018). Damage classification and derivation of damage probability matrices from L'Aquila (2009) post-earthquake survey data, *Bull. Earthq. Eng.* **16,** 3687–3720, doi: 10.1007/s10518-018-7600352-6.

Rota, M., A. Penna, and C. L. Strobbia (2008). Processing Italian damage data to derive typological fragility curves, *Soil Dynam. Earthq. Eng.* **28,** nos. 10/11, 933–947.

Silva, V., S. Akkar, J. Baker, P. Bazzurro, J. M. Castro, H. Crowley, M. Dolsek, C. Galasso, S. Lagomarsino, R. Monteiro, *et al.* (2019). Current challenges and future trends in analytical fragility and vulnerability modelling, *Earthq. Spectra* **35,** no. 4, 1927–1952, doi: 10.1193/042418EQS101O.

Slejko, D., G. B. Carulli, M. Riuscetti, F. Cucchi, S. Grimaz, A. Rebez, F. Accaino, A. Affatato, S. Biolchi, D. Nieto, *et al.* (2011). Soil characterization and seismic hazard maps for the Friuli Venezia Giulia region (NE Italy), *Boll. Geof. Teor. Appl.* **52,** 59–104.

Sugan, M., and L. Peruzza (2011). Seismic districts of Veneto, *Boll. Geof. Teor. Appl.* **52,** s3–s90, doi: 10.4430/bgta0057.

SYNER-G (2009). Deliverable 7.1—Functional fragility curve archive, available at http://www.vce.at/SYNER-G/pdf/deliverables/D7.01_Deliverable_7.1_FINAL.pdf (last accessed October 2020).

SYNER-G (2013). Reference Report 4—Guidelines for deriving seismic fragility functions of elements at risk: Buildings, lifelines, transportation networks and critical facilities, *Scientific and Technical Research series*, 250 pp., ISSN 1831-9424 (online), ISSN 1018-5593 (print), ISBN 78-92-79-28966-8, doi: 10.2788/19605.

Vona, M. (2014). Fragility curves of existing RC buildings based on specific structural performance levels, *Open J. Civ. Eng.* **4,** 120–134, doi: 10.4236/ojce.2014.42011.

Wald, D. J., V. Quitoriano, T. H. Heaton, H. Kanamori, C. W. Scrivner, and C. B. Worden (1999). TriNet "ShakeMaps": Rapid generation of peak ground-motion and intensity maps for earthquakes in Southern California, *Earthq. Spectra* **15,** 537–556, doi: 10.1193/1.1586057.

Wieland, M., M. Pittore, S. Parolai, and J. Zschau (2012). Exposure estimation from multi-resolution optical satellite imagery for seismic risk assessment, *ISPRS Int. J. Geo-Inform.* **1,** no. 1, 69–88.

Worden, C. B., E. M. Thompson, J. W. Baker, A. P. Brendon, N. Luco, and D. J. Wald (2018). Spatial and spectral interpolation of ground-motion intensity measure observations, *Bull. Seismol. Soc. Am.* **108,** 866–875, doi: 10.1785/0120170201.

Worden, C. B., E. M. Thompson, M. Hearne, and D. J. Wald (2020). ShakeMap manual online: Technical manual, user's guide, and software guide, *U.S. Geol. Surv.*, available at http://usgs.github.io/shakemap/ (last accessed October 2020), doi: 10.5066/F7D21VPQ.

Yepes-Estrada, C., V. Silva, T. Rossetto, D. D'Ayala, I. Ioannou, A. Meslem, and H. Crowley (2016). The global earthquake model physical vulnerability database, *Earthq. Spectra* **32,** no. 4, 2567, doi: 10.1193/011816EQS015DP.

Zelaschi, C., R. Monteiro, and R. Pinho (2019). Critical assessment of intensity measures for seismic response of Italian RC Bridge Portfolios, *J. Earthq. Eng.* **23,** no. 6, 980–1000, doi: 10.1080/13632469.2017.1342293.

Zucconi, M., R. Ferlito, and L. Sorrentino (2020). Validation and extension of a statistical usability model for unreinforced masonry buildings with different ground motion intensity measures, *Bull. Earthq. Eng.* **18,** 767–795, doi: 10.1007/s10518-019-00669-2.